Model Predictive Direct Torque Control of a Variable Speed Drive with a Five-Level Inverter

Tobias Geyer, *Member, IEEE*, and Georgios Papafotiou, *Member, IEEE*

***Abstract*—Model Predictive Direct Torque Control (MPDTC) is a newly developed computational control method for medium-voltage drives, which, based on the principles of Model Predictive Control, reduces the converter's switching losses and improves the torque's Total Harmonic Distortion (THD) with respect to standard Direct Torque Control (DTC), while maintaining DTC's favorable dynamic and robustness properties. In this paper, MPDTC is adapted and applied to a five-level converter driving a high frequency induction machine. This application poses the challenge to produce five-level waveforms within the (short) fundamental period while respecting the converter's thermal limitations. The MPDTC methodology is tailored to the specific application by decomposing the controller into a machine and three phase controllers. Initial results suggest that, with respect to Pulse Width Modulation (PWM), MPDTC is capable of simultaneously reducing the switching losses and the torque THD, both by roughly 50 %.**

I. Introduction

Medium-voltage variable speed drives have evolved into reliable solutions for the controlled operation of electric motors. In the power range of one to twenty megawatts (MW), multi-level topologies based on Integrated Gate Commutated Thyristors (IGCT) are predominantly used as power electronic converters. These include the three-level Neutral Point Clamped (NPC) topology of ABB's ACS 6000 medium-voltage drive, and the five-level topology of the ACS 5000 model, which is based on series connected three-level H-bridges. These drives cover typical medium-voltage applications such as metal rolling mills, fans and blowers in the power generation industry, pumps for water treatment installations and compressors for oil and gas applications.

Of the various methods developed for the control of medium-voltage drives, Direct Torque Control (DTC) stands out for its excellent dynamic response and its robustness with respect to uncertainties in the motor parameters [1], [2]. The control problem in DTC entails the selection, at discrete time instants, of the suitable converter switch combinations that, by applying the corresponding voltages to the machine terminals, maintain the torque and the amplitude of the stator flux of the motor within pre-specified hysteresis bounds. Additionally, in multi-level topologies, the control problem also includes balancing the converter's neutral point potential(s). Typically, DTC in medium-voltage applications is tuned (by the proper selection of the hysteresis bounds) to feature an average switching frequency of approximately 250 Hz, the latter figure stemming from the thermal limitations of the available semiconductors and the existing cooling concepts.

This paper focuses on the control problem of the ACS 5000 drive system's five-level topology driving a high frequency induction motor with a fundamental frequency of almost 200 Hz. Compared to the standard 50 Hz case, the switching pattern generation for the significantly shorter fundamental period becomes a challenge in the face of the above mentioned switching frequency limitation, thus motivating the investigation of alternative schemes. One obvious solution is to use modulation-based methods, such as control schemes employing standard carrier-based Pulse Width Modulation (PWM) [3] or Optimal Pulse Patterns (OPP), see e.g. [4]. Contrary to these approaches, in this paper, we propose Model Predictive DTC (MPDTC) for the ACS 5000 and benchmark it to a PWM scheme.

In the newly developed MPDTC concept, novel ideas from the area of hybrid systems (mixed integer linear systems) and Model Predictive Control (MPC) [5], [6] were adopted to address the DTC control problem of medium-voltage motor drives. Specifically, the goal is to reduce the switching frequency and/or the switching losses of the inverter, while keeping the drive's controlled variables (airgap torque, stator flux and neutral point potential) within their bounds and maintaining the favorable dynamic properties of standard DTC. In [7], [8], the MPDTC concept is presented in detail for the case of an induction motor drive with a three-level NPC inverter, and [9] provides experimental results with a 2.5 MVA machine that verify the simulation results with a high degree of accuracy. The MPDTC algorithm is generalized in [10] and the minimization of the switching losses (rather than the switching frequency) is addressed in [10] and [11]. A more detailed literature study is available in [7] and [8].

In this paper, the generalized MPDTC framework is applied to the ACS 5000 topology with the goal of more efficiently operating the converter driving the high frequency machine by reducing the switching losses and by improving the torque THD. After discussing the physical setup of the drive in Section II, Section III states the control objectives, and Section IV presents the hierarchical MPDTC algorithm with its machine and the three phase controllers. Simulation results are presented in Section V to benchmark the performance of MPDTC with respect to PWM. Section VI concludes the paper.

II. Drive System

A. Physical Model of the Drive System

The ACS 5000 is a medium-voltage ac-ac drive system that features a 36-pulse diode rectifier for the ac-dc conversion and a voltage source converter (VSC) for the dc-ac conversion. Between the two stages are three independent and floating dc-links, one for each phase. As shown in Fig. 1, each phase of the VSC comprises a three-level H-bridge module, the detailed schematic of which is given in Fig. 2. Each phase module consists of two legs, while each leg in turn consists of four IGCTs,

T. Geyer is currently with the Department of Electrical and Computer Engineering, The University of Auckland, New Zealand, t.geyer@ieee.org

G. Papafotiou is with ABB Corporate Research, 5405 Baden-Dättwil, Switzerland, georgios.papafotiou@ch.abb.com

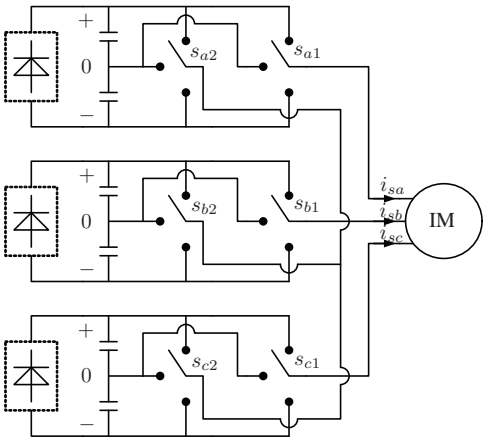

Fig. 1: Simplified topology of the ACS 5000 drive system, where IM refers to the high-frequency induction machine

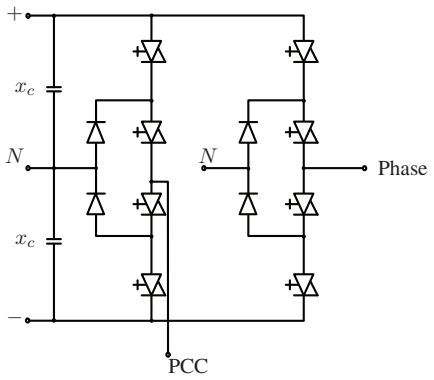

Fig. 2: Topology of one of the three phase modules. Each phase module is an H-bridge with a floating dc-link fed by a diode rectifier. The right leg's central point is connected to one of the motor phases, while the left leg's central point is connected to the point of common coupling (PCC)

four freewheeling diodes (which are not shown for simplicity) and two NPC diodes. Each leg is capable of connecting its central point to three different potentials: the positive rail, the negative rail, and the neutral point of the corresponding dc-link. Hence, a total of $3^2 = 9$ switch positions exist for each phase module. These switch positions can be fully described by the integer variables $s_i = [s_{i1}\ s_{i2}]^T \in \{0, \pm 1\}^2$, where s_{i1} and s_{i2} describe the switch positions of the module's right and left leg, respectively, and $i \in \{a, b, c\}$ denotes the phase.

The three-phase connection of the VSC is realized by connecting the right leg's central point of each phase module to the corresponding motor phase, while the left leg's central point is connected to the point of common coupling. As a result, the difference between the central point's two potentials is the phase voltage as seen from the motor side, which can take five different values, namely $-2V_{\text{dc}}, -V_{\text{dc}}, 0, V_{\text{dc}}, 2V_{\text{dc}}$. This in turn implies that the phase voltages of the VSC topology can be described by the integer variable $u = [u_a\ u_b\ u_c]^T \in \{0, \pm 1, \pm 2\}^3$. Note that the number of possible (output) phase voltages, which is five, is smaller than the number of possible switch positions of the phase module, which is nine. This is due to the so called single phase redundancy, where certain phase voltages can be produced by more than one phase module switch position. More specifically, each of the phase voltages $-V_{\text{dc}}$ and V_{dc} can be obtained in two different ways, while the phase voltage zero can be built in three ways as summarized in Table I.

For the operation of the phase modules, the potential of the three neutral points deserves particular attention. The phase module's neutral point potential depends on the state of charge of its two dc-link capacitors. The potential is only affected when current is drawn directly from it, i.e. when exactly one of the leg's switch positions is zero (see also Table I). The neutral point potential of the i-th phase module is defined as $\upsilon_{ni} = 0.5(V_{\text{dc},i2} - V_{\text{dc},i1})$, with $V_{\text{dc},i1}$ and $V_{\text{dc},i2}$ being the upper and the lower dc-link voltages, respectively. Dynamically, υ_{ni} is described by

$$\frac{d\upsilon_{ni}}{dt} = -\frac{1}{2x_c}(|s_{i2}| - |s_{i1}|)i_{si}\,, \tag{1}$$

with i_{si} being the phase i stator current and x_c is one of the two symmetric capacitors of the dc-link.

u_i	$s_i = [s_{i1}\ s_{i2}]^T$	influence on υ_{ni}
2	$[1\ -1]^T$	no
1	$[0\ -1]^T$, $[1\ 0]^T$	yes
0	$[-1\ -1]^T$, $[0\ 0]^T$, $[1\ 1]^T$	no
-1	$[-1\ 0]^T$, $[0\ 1]^T$	yes
-2	$[-1\ 1]^T$	no

TABLE I: Relation between the phase switch position u_i and the corresponding H-bridge switch position s_i, where $i \in \{a, b, c\}$ denotes the phase. The third column indicates whether the choice of s_i has an influence on the neutral point potential υ_{ni}

B. Constraints on the Switch Transitions

Due to the existence of three independent phase modules, constraints on the switch transitions arise only within the phase modules, but not between them. Specifically, in a phase module, each leg can switch only by at most one voltage level and switching needs to occur in the opposite halves of the module. For example, from the switch position $s_i = [-1\ 1]^T$, switching is only admissible to $[-1\ 0]^T$, $[0\ 1]^T$ and $[0\ 0]^T$ (but not to any of the other five switch positions). Fig. 3 depicts the allowed switch transitions per phase module. As a result, considering the i-th phase switch position u_i, switching is admissible only between the pairs $-2 \leftrightarrow -1$, $-1 \leftrightarrow 0$, $0 \leftrightarrow 1$, $1 \leftrightarrow 2$, $-2 \leftrightarrow 0$ and $0 \leftrightarrow 2$. The number of admissible switch transitions between H-bridge switch positions s is thus upper bounded by $7^3 = 343$, while for transitions between phase switch positions u this number is with $5^3 = 125$ almost a third. This fact motivates the hierarchical control architecture to be proposed in Section IV.

C. Switching Losses

The drive's converter comprises three kinds of semiconductors, namely GCTs, freewheeling diodes, and NPC diodes. In the case of GCTs, one needs to distinguish between turn-on and turn-off losses, while for the diodes only the reverse recovery losses are of significance, which, for simplicity, will be assumed to be the same for both the freewheeling and the NPC diodes.

For the GCTs, the switch-on and -off energy losses can be well approximated to be linear both in the voltage and in the phase current. Since the voltage seen by each semiconductor is

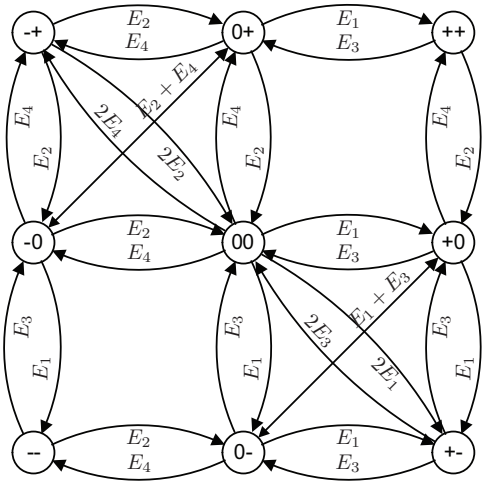

Fig. 3: Switch combinations $s_i = [s_{i1}\ s_{i2}]^T$ in a 3-level H-bridge along with the allowed switch transitions and the associated switching losses assuming a positive phase current i_{si}

always half the total dc-link voltage (assuming a well-balanced neutral point), the losses can be calculated using the formulas

$$E_{\text{on}} = e_{\text{on}} \frac{1}{2} V_{\text{dc}}\, i_{\text{ph}}\,, \quad E_{\text{off}} = e_{\text{off}} \frac{1}{2} V_{\text{dc}}\, i_{\text{ph}}\,, \tag{2}$$

where e_{on} and e_{off} are coefficients characterizing the semiconductor, and i_{ph} is the phase current. For the diodes, the reverse recovery losses are linear in the voltage, but nonlinear in the current.

$$E_{\text{rr}} = e_{\text{rr}} \frac{1}{2} V_{\text{dc}}\, f_{\text{rr}}(i_{\text{ph}})\,, \tag{3}$$

where e_{rr} is a coefficient for the reverse recovery losses. Usually, the nonlinear function $f_{\text{rr}}(\cdot)$ is not exactly known and one needs to resort to experimental data.

These formulas can be simplified by noting that the predictive algorithm only requires the comparison of the switching losses of the different switching scenarios (rather than the specific value of the losses themselves). Assuming roughly the same dc-link voltage in all phase modules, the term $\frac{1}{2}V_{\text{dc}}$ can be thus removed from the above equations.

Based on this, switching maps can be built that depict the current-dependent switching losses for each admissible switch transition of a phase module. Two such maps are required – one for positive and one for negative phase currents. In Fig. 3, such a map is depicted for a 3-level H-bridge assuming a positive phase current, where $E_1 = E_{\text{on}} + E_{\text{rr}}$, $E_2 = E_{\text{on}} + 2E_{\text{rr}}$, $E_3 = E_{\text{off}}$ and $E_4 = E_{\text{off}} + E_{\text{rr}}$. These losses are the total losses per phase module, i.e. the sum of the losses in the left and in the right phase leg. As an illustrative example of how the switching losses are derived consider Fig. 4.

III. Control Problem

The control problem of a variable speed drive in the megawatt range is complex with multiple, conflicting objectives. With respect to the machine, in standard DTC, the electromagnetic torque and the length (or magnitude) of the stator flux are to be kept within given (hysteresis) bounds and controlled dynamically with short transients. In MPDTC, these objectives are inherited from DTC. In addition, in order to reduce the losses in the machine and to avoid problems with the mechanical load (wear of the shaft and the possible

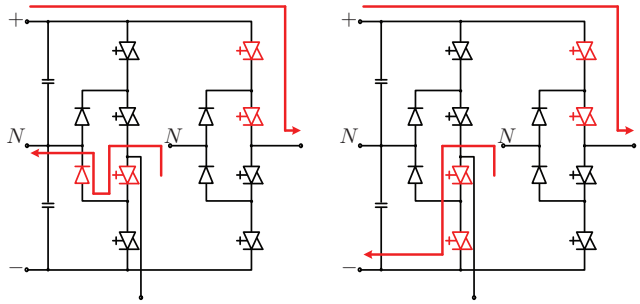

Fig. 4: Commutation from $s_i = [1\ 0]^T$ to $[1\ -1]^T$. For a positive phase current, this entails the switching loss $E_1 = E_{\text{on}} + E_{\text{rr}}$

excitation of eigenfrequencies of the load) the torque THD needs to be also minimized.

The inverter, on the other hand, has a limited thermal cooling capability thus limiting the total losses that can be tolerated without destroying the semiconductor switching devices. Thus the losses, particularly the switching losses, in the inverter are to be minimized. Apart from that, the three neutral point potentials need to be balanced around zero.

IV. Model Predictive Direct Torque Control

A. Model Predictive Control

In MPC [5], the current control input is obtained by solving at each sampling instant a constrained optimal control problem based on the predictions provided by an internal model of the controlled process. The optimal control problem is formulated over a finite or infinite horizon using the current state of the plant as initial state. The underlying optimization procedure yields an optimal control sequence that minimizes a given objective function. Only the first control input of this sequence is applied in accordance with the so called receding horizon policy. At the next sampling instant, the control sequence is recomputed over a shifted horizon, thus providing feedback.

B. Internal Controller Model

The internal controller model is an integral part of the MPDTC scheme. Plainly speaking, the model provides MPDTC with the ability to look into the future by predicting the drive's response to different switching sequences. More precisely, the model's purpose is to predict the trajectories of the electromagnetic torque and the stator flux over several sampling intervals in an open-loop fashion. Unlike in [8], only the dynamics of the motor are modelled, while a dynamical model of the neutral point potentials is not required here.

Due to space limitations, the detailed model derivation, which can be found in [7] and [8], is omitted here and only a summary of the controller model is provided. Assuming a constant rotor speed within the prediction horizon, and modelling the induction motor in the stationary $\alpha\beta$ reference, four machine states $x \in \mathbb{R}^4$ result. The three neutral point potentials are described by the state vector $z = [v_{na}\ v_{nb}\ v_{nc}]^T$. The model's input vector are the switch positions $u = u_{abc} = [u_a\ u_b\ u_c]^T \in \{0, \pm 1, \pm 2\}^3$, while the electromagnetic torque T_e and the length of the stator flux Ψ_s constitute the output vector $y = [T_e\ \Psi_s]^T$. The model is formulated in the discrete-time domain with a sampling interval of $T_s = 25\,\mu s$, which is typical for DTC.

Machine controller:	
Objective:	Keep the torque and the stator flux magnitude within the given bounds and minimize the switching losses
Algorithm:	MPDTC
Inputs:	$x(k)$, $u(k-1)$
Output:	$u(k)$
Phase controller for the i-th H-bridge, with $i = \{a, b, c\}$:	
Objective:	Balance the neutral point potential around zero
Algorithm:	Comparator logic
Inputs:	$z_i(k)$, $u_i(k)$
Output:	$s_i(k)$

TABLE II: Decomposition of the controller into a machine controller and three phase controllers, where $x \in \mathbb{R}^4$ and $z_i \in \mathbb{R}$, $i = \{a, b, c\}$, are the machine and the i-th inverter state, respectively, while $u = [u_a\ u_b\ u_c]^T \in \{0, \pm 1, \pm 2\}^3$ and $s_i = [s_{i1}\ s_{i2}]^T \in \{0, \pm 1\}^2$ are the phase switch positions and the H-bridge switch positions, respectively

C. Machine Controller

To greatly reduce the computational burden, the MPDTC is tailored to the ACS 5000 topology by decomposing the controller into a machine controller and three phase controllers as summarized in Table II. To facilitate the controller decomposition, it is expedient to remove the $[1\ 1]^T$ and the $[-1\ -1]^T$ H-bridge switch positions. Note that these switch positions cannot be used for the balancing of the neutral point potential. Moreover, a detailed analysis, which is beyond the scope of this paper, shows that the expected impact on the total switching losses is less than $4\,\%$.

The main controller is based on MPDTC [7], [8], which is generalized in [10]. While respecting the constraints on the switch transitions shown in Section II-B, this controller maintains the torque and the magnitude of the stator flux between the hysteresis bounds by choosing the phase switch position u, or equivalently the voltage vector seen by the machine. Simultaneously, the controller minimizes the switching losses by using the model derived in Section II-C. Strictly speaking, the H-bridge switch positions s_i are required for the computation of the switching losses rather than only the phase switch positions u_i. Yet, given that the H-bridge switch positions $[-1\ -1]^T$ and $[1\ 1]^T$ are not considered, unique switching losses can be directly associated with the phase switch transitions. This becomes evident from Fig. 3. As an example, consider switching from $u_i = 2$ to $u_i = 1$, which is equivalent to switching from $s_i = [-1\ 1]^T$ to $s_i = [-1\ 0]^T$ or $[0\ 1]^T$. In both cases, the incurred switching losses are E_2.

Starting at the current time-step k, the generalized MPDTC algorithm [10] iteratively explores the tree of feasible switching sequences forward in time. For these switching sequences, the internal controller model is used to compute the torque and flux response, i.e. the output trajectories. At each intermediate step, all switching sequences must yield output trajectories that are either *feasible*, or *pointing in the proper direction*. We refer to these switching sequences as *candidate* sequences. Feasibility means that the output variable lies within its corresponding bounds; pointing in the proper direction refers to the case in which an output variable is not necessarily feasible, but the degree of the bounds' violation decreases at every time-step within the switching horizon. The above conditions need to hold *componentwise*, i.e. for both output variables.

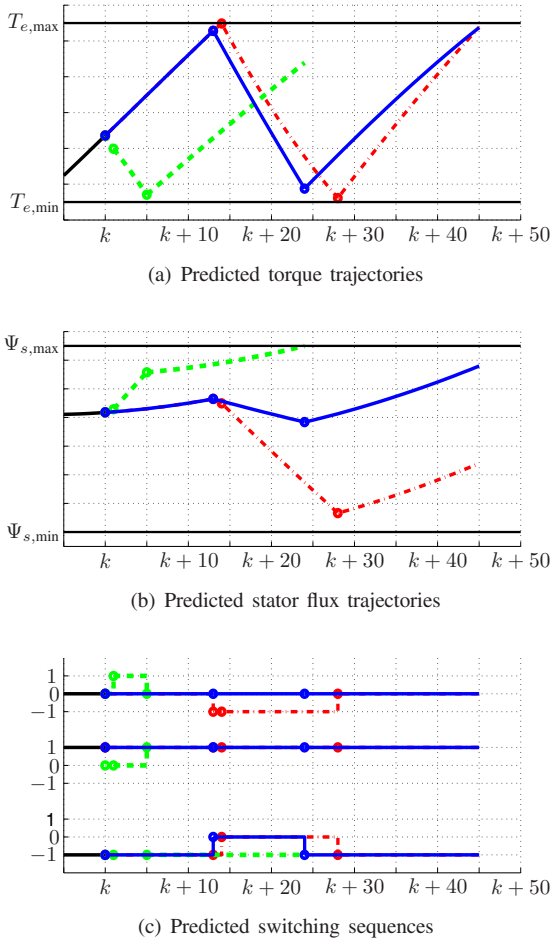

(a) Predicted torque trajectories

(b) Predicted stator flux trajectories

(c) Predicted switching sequences

Fig. 5: Assuming the switching horizon 'eSSESE' and a three-level inverter, three candidate switching sequences are shown with their associated torque and stator flux trajectories between their respective upper and lower bounds. The time-axis is given by the sampling instants with the sampling interval $T_s = 25\,\mu$s.

The traversing through the tree is controlled by the so called *switching horizon* composed of the elements 'S' and 'E', which stand for 'switch' and 'extrapolate' (or more generally 'extend'), respectively. The switching horizon, with its upper bound on the number of switch transitions and extension steps, can be considered as an alternative to a (fixed) prediction horizon in time. Note that for MPDTC, the resulting prediction horizon is of variable length in time. As an example for a switching horizon, consider 'SSESE', which stands for switching at time-steps k and $k+1$ and subsequently extending the trajectories until one or more output trajectory ceases to be feasible and/or pointing in the proper direction. Assume this happens at time-step $k + \ell$ thus triggering the third switching event that is followed by another extension step. We use the task 'e' to add an optional extension leg to the switching horizon. Using 'eSSESE' as an illustrative example, three candidate switching sequences are depicted in Fig. 5 along with their output trajectories. Note that in this example, the controller anticipates three switch transitions and looks tens of time-steps into the future, while standard DTC considers only one switch transition and looks only one step ahead.

Next, for each candidate switching sequence, the short-term average switching (power) losses are evaluated by computing

$u_i(k)$	$u_i(k-1)$	$p_i(k)$	$s_i(k)$
2			$[1\ -1]^T$
1	1		$s_i(k-1)$
1	$\neq 1$	1	$[0\ -1]^T$
1	$\neq 1$	-1	$[1\ 0]^T$
0			$[0\ 0]^T$
-1	-1		$s_i(k-1)$
-1	$\neq -1$	1	$[0\ 1]^T$
-1	$\neq -1$	-1	$[-1\ 0]^T$
-2			$[-1\ 1]^T$

TABLE III: The phase controller for the i-th H-bridge, which runs a simple comparator logic with $p_i = \text{sign}(i_{si})\text{sign}(v_{ni})$

the associated cost function E/n. In here, E denotes the switching (energy) losses, which are computed according to Section II-C, and n is the variable-length prediction horizon. The latter is the length of the predicted sequence (number of discrete time-steps). For the three switching sequences in Fig. 5, for example, n is 23, 44 and 45, respectively. Note that, to compute the losses, the phase currents need to be derived, which are linear combinations of the flux components, thus making this a computationally simple operation.

Last, in the optimization step, the switching sequence with the minimal cost is chosen. From this sequence, the first switch position $u(k)$ is selected and passed on to the three phase controllers.

D. Phase Controller

Each of the three H-bridges (phase modules) is controlled by its own phase controller that translates the respective phase switch position into switch positions of the H-bridge's two legs, e.g. for phase a, $u_a(k)$ is translated into $s_{a1}(k)$ and $s_{a2}(k)$. By exploiting the redundancies of the H-bridge switch positions, the local neutral point potential is balanced around zero without introducing any additional switch transitions. Note that the phase controllers are decoupled from each other.

The simplest version of a phase controller is the following algorithm, which is summarized in Table III. If the phase switch position remains unchanged, keep the H-bridge switch position. Else, if the new phase switch position is ± 1, balance the neutral point potential. The phase switch position $u_i = 1$ for example, can be realized in two ways. Assuming a positive phase current, $s_i = [1\ 0]^T$ ($[0\ -1]^T$) will decrease (increase) the neutral point potential. For a positive neutral point potential v_{ni}, the controller would translate $u_i = 1$ into $s_i = [1\ 0]^T$.

V. Performance Evaluation

This section shows simulation results of the proposed MPDTC scheme and benchmarks it with respect to a standard PWM approach. The comparison is made based on the ACS 5000 drive system with a 6.3 kV and 188.7 Hz induction machine rated at 12 MVA. The detailed parameters can be found in Table IV. For this comparison, a very accurate and detailed Matlab/Simulink model of the drive is used, which was provided by ABB to ensure as realistic a simulation set-up as possible. The induction motor model includes the saturation of the machine's magnetic material and the changes of the rotor resistance due to the skin effect. For MPDTC, the Simulink block with the control strategy is replaced by a function that runs the MPDTC algorithm at each sampling instant. The

Induction motor	Voltage	6294 V	r_s	0.0024 p.u.
	Current	1101 A	r_r	0.0097 p.u.
	Real power	8 MW	x_{ls}	0.1437 p.u.
	Apparent power	12 MVA	x_{lr}	0.0054 p.u.
	Frequency	188.7 Hz	x_m	4.3251 p.u.
	Rotational speed	11200 rpm		
Inverter	Dc-link voltage	5184 V	V_{dc}	1.009 p.u.
			x_c	30.523 p.u.

TABLE IV: Rated values (left) and parameters (right) of the drive

significance of such simulations is underlined by the very close match between previous simulations and experimental results using a very similar model – the simulation results in [8] predicted the experimental results in [9] accurately to within a few percent.

By selecting the MPDTC lower and upper torque bounds to be 0.85 and 1.15, and correspondingly setting the flux bounds at 0.94 and 1.03, the results summarized in Table V are achieved. Both, the PWM and the proposed MPDTC scheme were simulated for 1 s each. Subsequently, we place our focus on two important aspects of the drive's behavior, namely the actual semiconductor switching losses that reflect the thermal stresses on the converter and the motor torque THD that provides an indication of the machine losses. Specifically, the simulation results indicate that MPDTC is capable of simultaneously reducing both the switching losses and the torque THD by 50% when compared to the PWM scheme. While at a first glimpse, this result may seem to be contradictory, it can be explained by an inspection of the waveforms. For the PWM scheme, Fig. 6 shows the torque, the three neutral point potentials and the phase switch positions u_a, u_b, u_c along with the respective stator currents i_{sa}, i_{sb}, i_{sc}. All quantities are given in p.u. and the trajectories are plotted over a time-frame of 10 ms.

Fig. 7 shows the corresponding plots for MPDTC with the switching horizon 'eSESE' and the above noted bounds. It can be seen that the torque ripple is more than halved, which is reflected in the significantly lower torque THD. The stator flux magnitude, which is not shown here, is more tightly controlled around its reference (which is one) by MPDTC leading to a reduction of the flux THD by 20 % with respect to the PWM scheme. In both cases, the neutral point potentials are well balanced around zero.

The resulting (phase) switching pattern differs significantly between the two control schemes. Due to its fixed carrier frequency, the PWM scheme switches each phase continuously with half the carrier frequency. In particular, multiple switch transitions occur when the phase currents are close to their peak values. In contrast to that, MPDTC requires only about half of the switch transitions, while tending to reduce excessive

Control scheme	Horizon	reduction in percent w. r. t. PWM P_{loss}	f_{sw}	$T_{e,\text{THD}}$	$T_{e,\text{ripple}}$
PWM	–	0	0	0	0
MPDTC	eSE	56	49	49	64
MPDTC	eSESE	60	52	52	67

TABLE V: Benchmarking of MPDTC with respect to the PWM scheme. The percentage-wise reduction with respect to PWM is shown for the switching losses P_{loss}, the switching frequency f_{sw}, the torque THD $T_{e,\text{THD}}$ and the torque ripple $T_{e,\text{ripple}}$. The operating point is at 90 % speed and 100 % torque

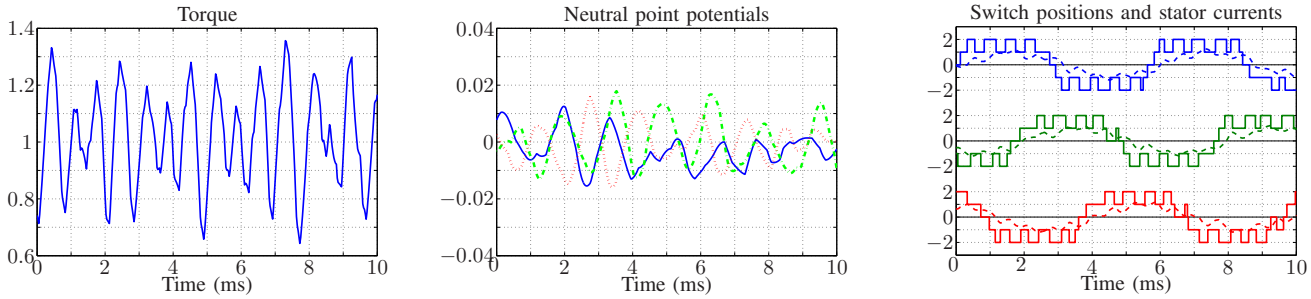

Fig. 6: Steady-state operation at 90 % speed and 100 % torque for the PWM scheme. All quantities are given in p.u.

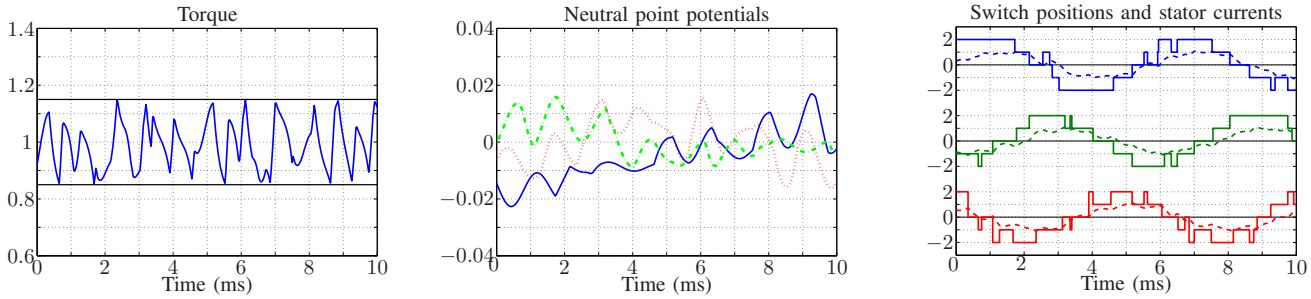

Fig. 7: Steady-state operation at 90 % speed and 100 % torque for MPDTC with the switching horizon 'eSESE'. All quantities are given in p.u.

switching at high current values. This characteristic results from incorporating the switching loss model in the MPDTC algorithm and by formulating the objective function accordingly to penalize the short-term average switching power.

An interpretation of why, for this specific topology, MPDTC seems to outperform the traditional PWM controller and how it achieves at the same time to both improve the torque THD and reduce the switching losses, might be the following. Firstly, by exploring the tree of admissible switching sequences, MPDTC can take advantage of the redundancies in the phase switch positions (note that, for a five-level inverter, up to five phase switch positions lead to the same phase voltage seen by the machine). Secondly, the internal controller model and the losses model enable the controller to look into the future by predicting the effect of the possible switching sequences, while the objective function defines the optimality criterion based on which the optimal switch position is chosen. Thirdly, in contrast to classic motor control schemes, MPDTC considers both the torque and the stator flux simultaneously in a Multiple Input Multiple Output (MIMO) control approach.

VI. Conclusion

In this paper, we proposed a Model Predictive DTC algorithm tailored to the five-level topology of the ACS 5000. Without any doubt, the computational burden of this algorithm is high. Yet, as the successful implementation of MPDTC on the ACS 6000 and subsequent test runs demonstrate [9], the computational demand of such algorithms can be accommodated by modern control platforms. Apart from that, the performance improvements with respect to PWM schemes are promising. Even though only simulation results were provided, simulations using a very similar simulation setup were very accurately verified by experimental results [9].

Acknowledgment

This work was supported by ABB Switzerland Ltd. The authors would like to thank Christian Stulz of ABB ATDD, Turgi, Switzerland, for his advice and support.

References

[1] I. Takahashi and T. Noguchi, "A new quick response and high efficiency control strategy for the induction motor," *IEEE Trans. Ind. Applicat.*, vol. 22, no. 2, pp. 820–827, Sep./Oct. 1986.

[2] G. S. Buja and M. P. Kazmierkowski, "Direct torque control of PWM inverter-fed AC motors – a survey," *IEEE Trans. Ind. Electron.*, vol. 51, no. 4, pp. 744–757, Aug. 2004.

[3] J. Holtz, "Pulsewidth modulation – a survey," *IEEE Trans. Ind. Electron.*, vol. 32, no. 5, pp. 410–420, Dec. 1992.

[4] N. Oikonomou, "Control of medium-voltage drives at very low switching frequency," Ph.D. dissertation, University of Wuppertal, 2008.

[5] C. E. Garcia, D. M. Prett, and M. Morari, "Model predictive control: Theory and practice – a survey," *Automatica*, vol. 25, no. 3, pp. 335–348, Mar. 1989.

[6] S. J. Qin and T. A. Badgwell, "A survey of industrial model predictive control technology," *Control Engineering Practice*, vol. 11, no. 7, pp. 733–764, Jul. 2003.

[7] T. Geyer, "Low complexity model predictive control in power electronics and power systems," Ph.D. dissertation, Automatic Control Laboratory ETH Zurich, 2005.

[8] T. Geyer, G. Papafotiou, and M. Morari, "Model predictive direct torque control - part I: Concept, algorithm and analysis," *IEEE Trans. Ind. Electron.*, vol. 56, no. 6, pp. 1894–1905, Jun. 2009.

[9] G. Papafotiou, J. Kley, K. G. Papadopoulos, P. Bohren, and M. Morari, "Model predictive direct torque control - part II: Implementation and experimental evaluation," *IEEE Trans. Ind. Electron.*, vol. 56, no. 6, pp. 1906–1915, Jun. 2009.

[10] T. Geyer, "Generalized model predictive direct torque control: Long prediction horizons and minimization of switching losses," in *Proc. IEEE Conf. on Decision and Control*, Dec. 2009.

[11] S. Mastellone, G. Papafotiou, and E. Liakos, "Model predictive direct torque control for MV drives with LC filters," in *Proc. European Power Electron. Conf.*, Barcelona, Spain, Sep. 2009.